Mon. Not. R. Astron. Soc. **000**, 000–000 (0000) Printed 3 August 2017 (MN LATEX style file v2.2)

# SDSS-IV MaNGA: Slow Rotators Quench Faster than Fast Rotators

R. J. Smethurst,[1] K. L. Masters,[2] C. J. Lintott,[3] A. Weijmans,[4] M. Merrifield,[1] S. J. Penny,[2] A. Aragón-Salamanca,[1], J. Brownstein,[5] K. Bundy,[6] N. Drory,[7], D. R. Law,[8] R. C. Nichol [2]

[1] *School of Physics and Astronomy, The University of Nottingham, University Park, Nottingham, NG7 2RD, UK*
[2] *Institute of Cosmology and Gravitation, University of Portsmouth, Dennis Sciama Building, Barnaby Road, Portsmouth, PO13FX, UK*
[3] *Oxford Astrophysics, Department of Physics, University of Oxford, Denys Wilkinson Building, Keble Road, Oxford, OX13RH, UK*
[4] *School of Physics and Astrononomy, University of St Andrews, North Haugh, St Andrews, Fife, KY169RJ, UK*
[5] *Department of Physics and Astronomy, University of Utah, 115 S. 1400 E., Salt Lake City, UT 84112, USA*
[6] *University of California, Santa Cruz, 1156 High St. Santa Cruz, CA 95064, USA*
[7] *McDonald Observatory, The University of Texas at Austin, 1 University Station, Austin, TX 78712, USA*
[8] *Space Telescope Science Institute, 3700 San Martin Drive, Baltimore, MD 21218, USA*

3 August 2017

**ABSTRACT**

We present a study of the star formation histories of fast and slow rotators identified in the MaNGA sample. We select those galaxies which lie below the star forming sequence and inspect their kinematic maps to identify quenching slow rotators. We then create a sample of quenching fast rotators which matched in stellar mass. This results in a total sample of 202 kinematically classified galaxies, which is agnostic to visual morphology. We use $u-r$ and $NUV-u$ colours from SDSS and GALEX and an existing inference package, STARPY to conduct a first look at the onset time and exponentially declining rate of quenching of these galaxies. An Anderson-Darling test on the distribution of quenching rates across the two kinematic populations reveals they are statistically distinguishable ($2.9\sigma$). We find that quenching is more likely to occur at a rapid rate ($\tau \lesssim 1$ Gyr) for slow rotators than for fast rotators of the same stellar mass, in agreement with theories suggesting slow rotators are formed in major mergers. Conversely, we find that fast rotators quench at a much wider range of rates, consistent with secular evolution, minor mergers, gas accretion and environmentally driven mechanisms. However we also find evidence for a subset of fast rotators quenching at the same rapid rates as in the slow rotator sample. We therefore discuss how the total gas mass of a merger, rather than the merger mass ratio, may decide a galaxy's ultimate kinematic fate.

**Key words:** galaxies – photometry, galaxies – statistics, galaxies – morphology

## 1 INTRODUCTION

Recent work studying the early-type (i.e. elliptical and lenticular) galaxy population has revealed that it is actually composed of two kinematically distinct populations. The majority of early-types are rotationally supported (Emsellem et al. 2011) with $\sim 7$ times the number of galaxies with kinematic discs ('fast' rotators), than those with either dispersion dominated kinematics ('slow' rotators) or kinematically decoupled cores (which, along with slow rotators are collectively referred to as 'non-regular' rotators; Cappellari et al. 2007; Emsellem et al. 2007). This has led to the proposal of a revision of Hubble's morphological classification scheme in the form of a 'comb' (see Figure 24 of Cappellari 2016), whereby the evolution of a galaxy, from disc to bulge-dominated, takes place along a 'tine' of the comb as a fast rotator, always retaining an underlying disc. If the discs of these regular rotators are destroyed, they then evolve along the 'handle' of the comb to become slow rotators.

Dry major mergers are considered the most likely process to produce high stellar mass slow rotators (Duc et al. 2011; Naab et al. 2014) as they can rapidly destroy the disc dominated nature of a galaxy (Toomre & Toomre 1972). Low stellar mass slow rotators (i.e. dwarf ellipticals with $M_* \lesssim 10^9\ M_\odot$) are thought to be formed via harassment mechanisms in the group and cluster environment (Toloba

et al. 2015). Fast rotators are thought to evolve from the slow build up of a galaxy's bulge over time, eventually overwhelming the disc. This growth is thought to occur via gas-rich major or minor mergers (Duc et al. 2011) and by gas accretion (Cappellari et al. 2013; Johnston et al. 2014) which can produce a bulge dominated but rotationally supported galaxy (which would be visually classified as an early-type in the Hubble classification scheme).

Both major mergers and minor mergers have been postulated as quenching mechanisms (Hopkins et al. 2008; Snyder et al. 2011; Hayward et al. 2014), with major mergers thought to cause a much faster quench of the remnant galaxy than a minor merger (Lotz et al. 2008, 2011). Gas accretion is also thought to cause quenching (albeit on longer timescales) due to the large gravitational potential of the bulge which builds as the accreted gas sinks to the centre of the galaxy. This prevents the disc from collapsing and forming stars in a process which is referred to as morphological quenching (Martig et al. 2009; Fang et al. 2013). Similarly, harassment is also thought to cause quenching through repeated high speed interactions with neighbouring galaxies which can strip both stars and gas from a galaxy and heat the gas needed for star formation (Knebe et al. 2006; Aguerri & González-García 2009). If fast and slow rotators form via these different mechanisms, we should therefore also expect to find a difference in the star formation histories of quenching or quenched fast and slow rotators.

This paper presents a first look at this problem by using an existing Bayesian star formation inference package, STARPY, to determine the quenching histories of a sample of quenching or quenched fast and slow rotators identified in the MaNGA sample, irrespective of visual morphology. We use broadband optical, $u-r$, and near-ultraviolet, $NUV-u$, colours from SDSS and GALEX to infer both the onset time and exponential rate of quenching for each galaxy. We aim to determine whether rotationally supported and dispersion dominated galaxies have different quenching histories.

This paper proceeds as follows. In Section 2 we describe our data sources and our Bayesian inference method for determining the quenching histories. We present our results in Section 3 and discuss the implications of these results in Section 4. The zero points of all magnitudes are in the AB system. We adopt the WMAP Seven-Year Cosmology (Jarosik et al. 2011) with $(\Omega_m,\ \Omega_\Lambda,\ h) = (0.26, 0.73, 0.71)$.

## 2 DATA AND METHODS

### 2.1 SDSS & GALEX Photometry

We use optical photometry from the Sloan Digital Sky Survey Data Release 7 (SDSS; York et al. 2000; Abazajian et al. 2009). We use the Petrosian magnitude, `petroMag`, values for the $u$ (3543Å) and $r$ (6231Å) wavebands provided by the SDSS DR7 pipeline (Stoughton et al. 2002). Further to this, we also required NUV (2267Å) photometry from the GALEX survey (Martin et al. 2005). Observed fluxes are corrected for galactic extinction (Oh et al. 2011) by applying the Cardelli, Clayton, & Mathis (1989) law. We also adopt $k$-corrections to $z = 0.0$ and obtain absolute magnitudes from the NYU-VAGC (Blanton et al. 2005; Padmanabhan et al. 2008; Blanton & Roweis 2007).

### 2.2 MaNGA Survey & Data Reduction Pipeline

MaNGA is a multi-object IFU survey conducted with the 2.5 m Sloan Foundation Telescope (Gunn et al. 2006) at Apache Point Observatory (APO) as part of SDSS-IV (Blanton et al. *submitted*). By 2020 MaNGA will have acquired IFU spectroscopy for $\sim 10000$ galaxies with $M_* > 10^9$ $M_\odot$ and an approximately flat mass selection (Wake et al. 2017). The target selection is agnostic to morphology, colour and environment.

In order to obtain spectra, MaNGA makes use of the Baryon Oscillation Spectroscopic Survey (BOSS) spectrograph (Smee et al. 2013). The BOSS spectrograph provides continuous coverage between 3600 $\mathring{A}$ and 10300 $\mathring{A}$ at a spectral resolution $R \sim 2000$ ($\sigma_{\rm instrument} \sim 77$km s$^1$ for the majority of the wavelength range[1]).

Complete spectral coverage to $1.5R_e$, a galaxy's effective radius, is obtained for the majority of targets; a subset have coverage to $2.5R_e$. See Bundy et al. (2015) for an overview of the MaNGA survey. For a further description of the instrumentation used by MaNGA see Drory et al. (2015). For a detailed description of the observing strategy see Law et al. (2015) and for a description of the survey design see Yan et al. (2016).

The raw data was processed by the MaNGA data reduction pipeline (DRP), which is discussed in detail in Law et al. (2016). The MaNGA DRP extracts, wavelength calibrates and flux calibrates all fibre spectra obtained in every exposure. The individual fibre spectra are then used to form a regular gridded datacube of $0.5''$ spaxels and spectral channels. The spectra are logarithmically sampled with bin widths of $\log\lambda = 10^{-4}$.

These datacubes are then analysed using the MaNGA data analysis pipeline (DAP); the development of which is ongoing and will be described in detail in Westfall et al. (in preparation). The primary output from the DAP are 2D "maps" (i.e., images) of measured properties, which include flux, stellar-continuum fits, stellar and gas kinematics, spectral index measurements, and absorption- and emission-line properties. The effective radius of a galaxy and the ellipticity within it, $\epsilon_e$, are provided for MaNGA galaxies in the NASA Sloan Atlas; we use the values measured with elliptical Petrosian apertures in `v1_0_1` of the catalogue provided in the SDSS Data Release 13 (SDSS Collaboration et al. 2016).

### 2.3 Data sample

Our galaxy sample is drawn from the 2,777 SDSS galaxies currently observed by the MaNGA survey, which make up the MaNGA DR14 data release (Abolfathi et al. 2017). We cross-matched these galaxies with a radius of $3''$ to the GALEX survey in order to obtain NUV photometry (see Section 2.1), resulting in 1,413 galaxies.

In this study we wish to investigate the quenching histories of galaxies, therefore we sub-select those galaxies which are below the star forming sequence (SFS). Here we use the global average star formation rates (SFR) quoted in the MPA-JHU catalogue (Kauffmann et al. 2003; Brinchmann

[1] Instrument resolution as a function of wavelength in shown in Figure 20 of Yan et al. (2016)

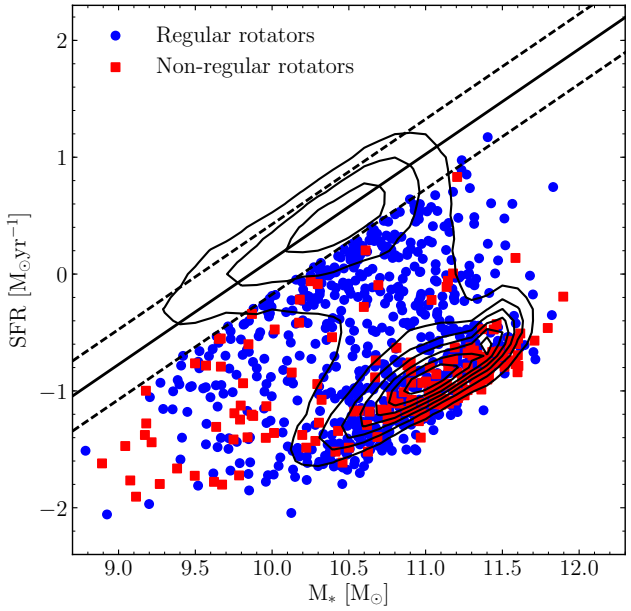


**Figure 1.** Stellar mass against star formation rate for the Q-MANGA-GALEX sample with regular (blue circles) and non-regular (red squares) rotators identified using Equation 2. Shown also are the contours for the entire MPA-JHU sample (black contours; i.e. SDSS DR7). The solid line shows the SFS as defined by Peng et al. (2010) at the average redshift of the Q-MANGA-GALEX sample, with $\pm1\sigma$ shown by the dashed lines. Note that the galaxies in the Q-MANGA-GALEX sample are chosen to be more than $1\sigma$ below the SFS as defined at their observed redshift and stellar mass (see Section 2.3).

et al. 2004, which are corrected for aperture bias). We do not use the MaNGA spectra to calculate SFRs since the bundles only extend to 1.5 $R_e$, therefore we may miss star formation occurring in the outer regions of galaxies which would result in an underestimate of the global SFR of a galaxy.

We select galaxies with a SFR more than $1\sigma$ below the SFS of Peng et al. (2010). Since we wish to test whether slow rotators quench at rapid rates, consistent with major mergers, we wish to include those galaxies which have just left the SFS (rather than only selecting those that are fully quenched, for example, $3\sigma$ below the SFS).

This selection on SFR when applied to the MANGA-GALEX sample results in a sample of 838 quenching or quenched galaxies, which we will refer to as the Q-MANGA-GALEX sample. This sample is shown in Figure 1.

In order to classify the galaxies in the Q-MANGA-GALEX sample as slow rotators or otherwise, we first calculate the specific stellar angular momentum as defined by Emsellem et al. (2007, 2011);

$$\lambda_{R_e} = \frac{\sum_{i=1}^{N} F_i \; R_i \; |V_i|}{\sum_{i=1}^{N} F_i \; R_i \; (V_i^2 + \sigma_i^2)^{1/2}}, \qquad (1)$$

where $F_i$ is the flux in the $i$th spaxel, $R_i$ the spaxel's distance from the galaxy centre (where $R_i < R_e$, the effective radius of a galaxy), $V_i$ the mean stellar velocity in that spaxel, $\sigma_i$ the stellar velocity dispersion in that spaxel and $N$ the total number of spaxels. In this work we use the *Python* function provided in the MaNGA DAP to calculate $\lambda_{R_e}$ using the values of mean flux, radius, stellar velocity and stellar velocity dispersion (corrected for instrumental resolution effects) provided for each spaxel of the data cube by the MaNGA DAP (see Section 2.2). Velocity dispersion measurements in each spaxel of a galaxy were confirmed to be above the instrument resolution of 77 km s$^{-1}$.

We then classify galaxies in the Q-MANGA-GALEX sample as non-regular rotators, or otherwise, using the definition from Cappellari (2016):

$$\lambda_{R_e} < 0.08 + \frac{\epsilon_e}{4} \qquad \text{with} \qquad \epsilon_e < 0.4. \qquad (2)$$

Both slow rotators and kinematically disturbed galaxies will satisfy this inequality, hence why this selection results ins a sample of non-regular rotators. Using this definition reveals 157 (19%) non-regular rotators and 673 (81%) regular rotators in the Q-MANGA-GALEX sample. Figure 2 shows the velocity maps of these galaxies plotted at their values of $\lambda_{R_e}$ and $\epsilon_e$, along with the definition of a non-regular rotator from Cappellari (2016) shown by the solid black line. Note the Q-MANGA-GALEX sample is agnostic to visual morphology, so our sample of regular rotators will contain both rotationally supported early-types and late-type galaxies.

The fraction of non-regular rotators found in the Q-MANGA-GALEX sample ($\sim 20\%$) is slightly higher than that found by previous works ($14 - 17\%$ of early-types in the ATLAS$^{3D}$ sample; Emsellem et al. 2011; Stott et al. 2016). Considering our sample is agnostic to visual morphology, we would expect a smaller fraction of non-regular rotators than previous works which specifically derived the fraction of non-regular rotators in a sample of early-types. However, other studies have shown that the non-regular rotator fraction increases with stellar mass (Cappellari et al. 2013), up to $\sim 90\%$ at $10^{12}$ M$_\odot$ (Veale et al. 2017). Upon inspection, the median stellar mass of the Q-MANGA-GALEX sample is $10^{10.8}$ M$_\odot$, which is in fact higher than the median stellar mass of the ATLAS$^{3D}$ sample at $10^{10.5}$ M$_\odot$, accounting for this apparent discrepancy.

In order to obtain a sample of slow rotators, one author (RJS) inspected the velocity maps of the 157 non-regular rotators identified in the Q-MANGA-GALEX sample to remove those galaxies which do not possess dispersion dominated kinematics. 56 galaxies exhibiting counter rotation or decoupled rotation were identified, example velocity maps for which are shown in the top row of Figure 3. This resulted in a sample of 101 slow rotators, example velocity maps for which are shown in the middle row of Figure 3.

In order to control for the degeneracies between mass, metallicity and dust (all of which can redden a galaxy's optical colour and mimic the effects of quenching) we selected a sub-sample of fast rotators from those identified as regular rotators in the Q-MANGA-GALEX sample. We matched to within $\pm$ 2.5 % of the stellar mass of each slow rotator to give 101 fast rotators, example velocity maps for which are shown in the bottom row of Figure 3. We shall refer to this combined sample of 202 fast and slow rotators as the MM-Q-MANGA-GALEX sample. An Anderson-Darling (AD) test reveals that the distribution of stellar masses of the fast rotators and slow rotators within this sample are statistically indistinguishable ($p = 0.25$). Similarly their redshift distributions are also statistically indistinguishable ($p = 0.10$).

We also consider the environmental densities of the fast and slow rotators by using estimates of the projected 5th nearest neighbour density, $\log \Sigma_5$, from Bamford et al.

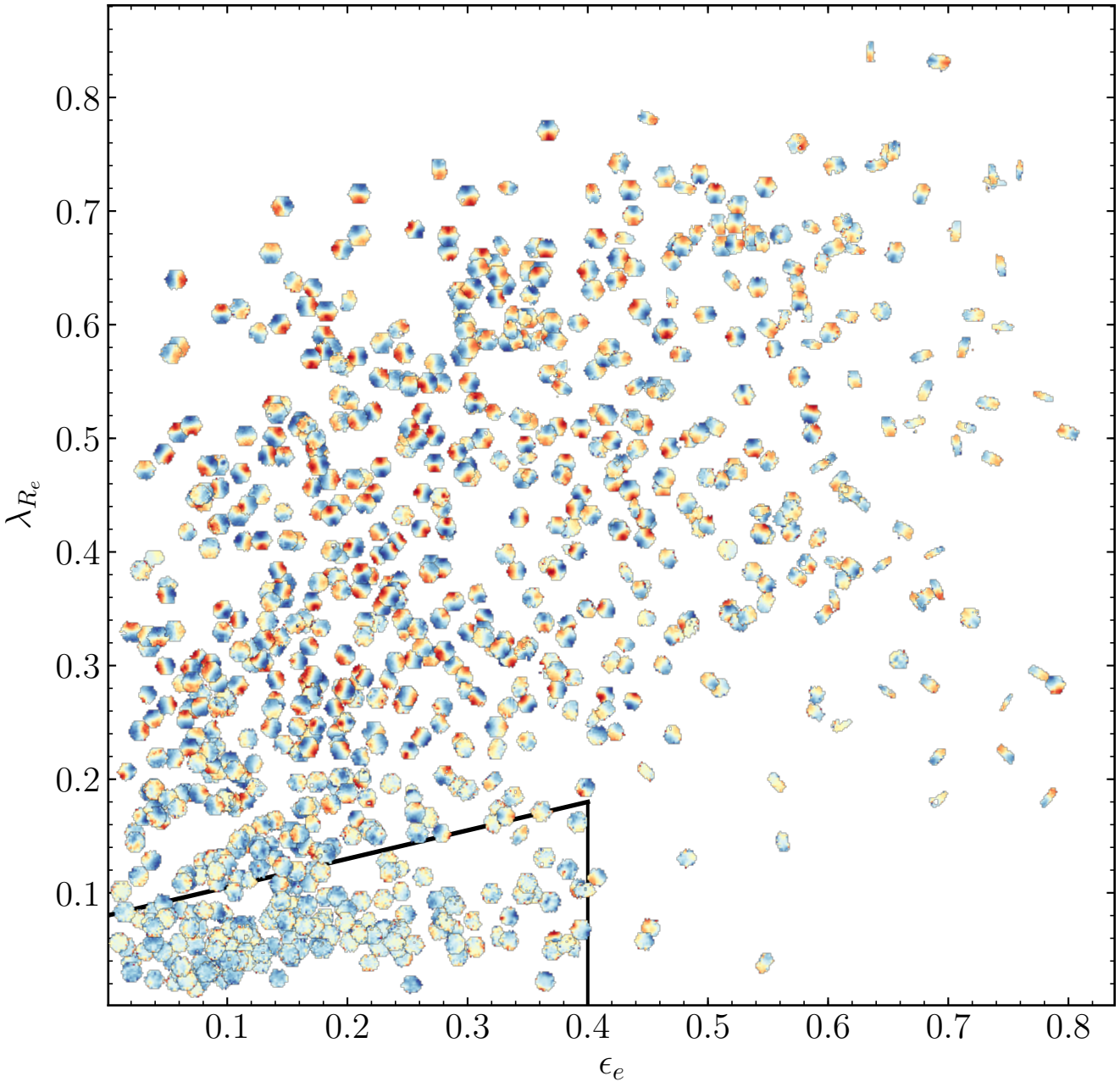


**Figure 2.** Ellipticity versus stellar angular momentum for the regular and non-regular rotators of the Q-MANGA-GALEX sample. Each point is shown by its stellar velocity map, each normalised to have a stellar velocity of 0 km s$^{-1}$ shown by the colour yellow. We show the separation between regular (i.e. fast) and non-regular rotators (i.e. slow rotators and objects with kinematically decoupled cores) from Cappellari (2016) with the solid black line.

(2009). An Anderson-Darling (AD) test reveals that the distribution of environment densities of the 77 slow rotators and 88 fast rotators of the MM-Q-MANGA-GALEX sample with $\log \Sigma_5$ measurements from Bamford et al. (2009) are statistically indistinguishable ($p = 0.23$).

This is surprising since the current theory is that slow rotators are more likely to be the central galaxy of a group or cluster, whereas fast rotators are more likely to be satellite galaxies (Cappellari et al. 2011; D'Eugenio et al. 2013; Houghton et al. 2013; Scott et al. 2014). Using the Yang et al. (2009) SDSS group catalogue we find similar fractions of the slow (76/98 of slow rotators with corresponding measurements in the Yang et al. group catalogue) and fast (71/99) rotators of the MM-Q-MANGA-GALEX sample are classified as their brightest group galaxy (BGG). However, these fractions include those galaxies which are isolated in their halos. Testing the distributions of the total group stellar mass for the fast and slow rotators we find a significant difference (AD test $p = 0.02$), with slow rotators residing in more massive groups.

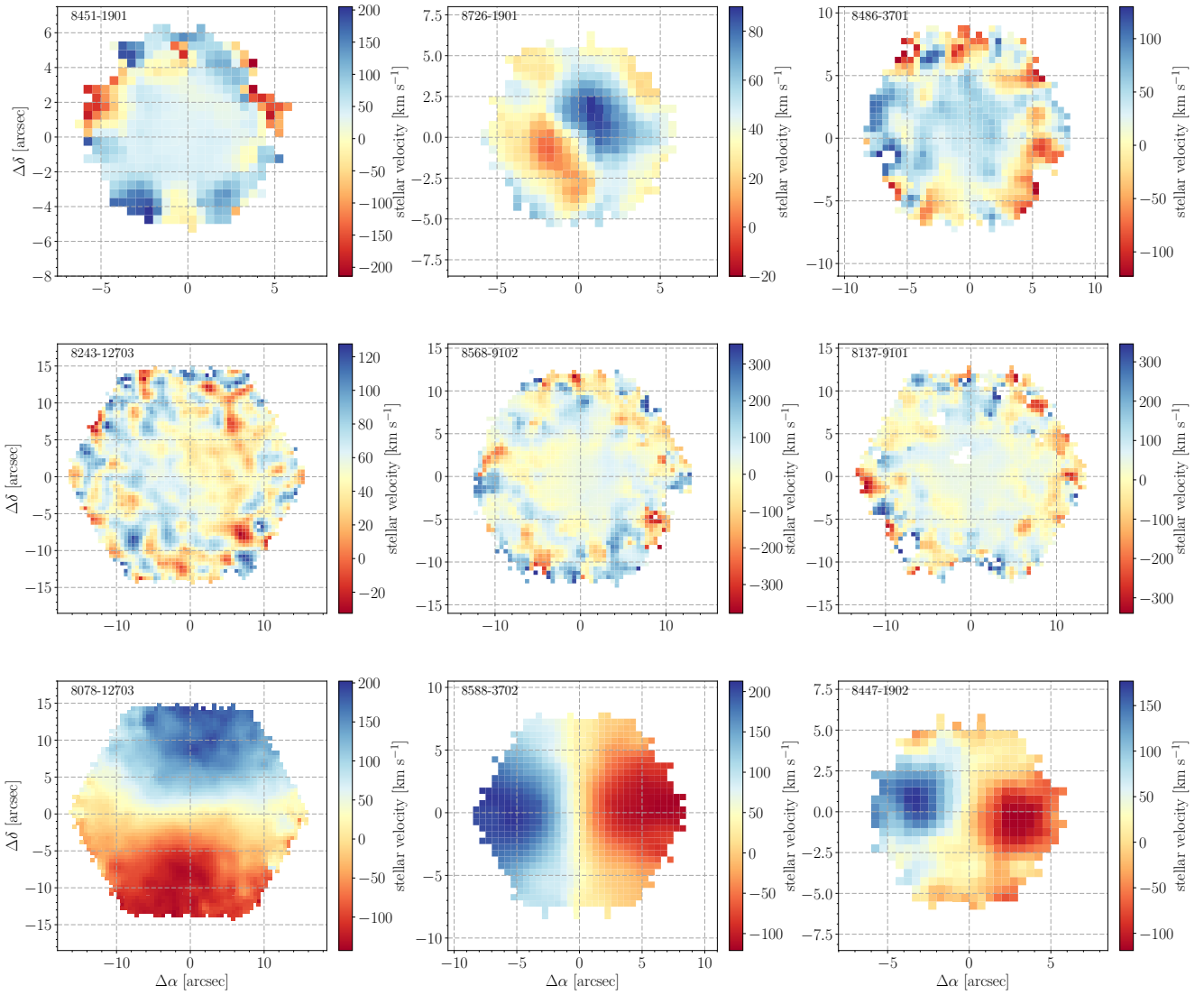


**Figure 3.** Example stellar velocity maps showing three galaxies removed from the non-regular rotator Q-MANGA-GALEX sample as their kinematics were not dispersion dominated (top row), three slow rotator galaxies with dispersion dominated kinematics (middle row), and three fast rotator galaxies with rotationally supported kinematics (bottom row). The MaNGA ID of each galaxy is shown in the top left of each panel.

If we then consider only those galaxies in groups with a total stellar mass greater than $10^{11}\mathrm{M}_{\odot}$ (under the simplifying assumption that this will remove the majority of single galaxy 'groups') we find the fraction of slow rotators classified as a BGG is 41/58 (71%), whereas for fast rotators this drops to 28/50 (56%), a statistically significant difference ($p = 0.0004$). Therefore, although the projected local environment densities of the two kinematic classes of galaxies are statistically indistinguishable, their positions within that given environment density do differ, as expected.

Given the above statistical tests, the only differences between the fast and slow rotators of the MM-Q-MANGA-GALEX sample is their kinematics, their colours and their position within their group halo. We can use the colours of the MM-Q-MANGA-GALEX sample to infer their star formation histories and compare the histories derived for slow and fast rotators.

### 2.4 Star Formation History Inference

STARPY[2] is a PYTHON code which allows the inference of the exponentially declining star formation history (SFH) of a single galaxy using Bayesian Markov Chain Monte Carlo techniques (Foreman-Mackey et al. 2013)[3]. The code uses the solar metallicity stellar population models of (Bruzual & Charlot 2003, hereafter BC03), assumes a Chabrier IMF (Chabrier 2003) and requires the input of the observed $u-r$ and $NUV-u$ colours and redshift. No attempt is made to model for intrinsic dust.

The SFH is described by an exponentially declining SFR described by two parameters; the time at the onset of quenching, $t_q$ [Gyr], and the exponential rate at which quenching occurs, $\tau$ [Gyr]. Under the simplifying assump-

[2] Publicly available: `http://github.com/zooniverse/starpy`
[3] `http://dan.iel.fm/emcee/`

tion that all galaxies formed at $t = 0$ Gyr with an initial burst of star formation, the SFH can be described as:

$$SFR = \begin{cases} i_{sfr}(t_q) & \text{if } t < t_q \\ i_{sfr}(t_q) \times exp\left(\frac{-(t-t_q)}{\tau}\right) & \text{if } t > t_q \end{cases} \quad (3)$$

where $i_{sfr}$ is an initial constant star formation rate dependent on $t_q$ (Schawinski et al. 2014; Smethurst et al. 2015). The simplifying assumption that all galaxies formed at $t = 0$ Gyr means that the age of each galaxy, $t_{\rm age}$, corresponds to the age of the Universe at its observed redshift, $t_{\rm obs}$. A smaller $\tau$ value corresponds to a rapid quench, whereas a larger $\tau$ value corresponds to a slower quench. A galaxy undergoing a slow quench is not necessarily quiescent by the time of observation. This SFH model has previously been shown to appropriately characterise quenching galaxies (Weiner et al. 2006; Martin et al. 2007; Noeske et al. 2007; Schawinski et al. 2014).

The probabilistic fitting methods to these star formation histories for an observed galaxy are described in full detail in Section 3.2 of Smethurst et al. (2015), wherein the STARPY code was used to characterise the morphologically dependence of the SFHs of $\sim 126,000$ galaxies. Similarly, in Smethurst et al. (2016), STARPY was used to show the prevalence of rapid, recent quenching within a population of AGN host galaxies and in Smethurst et al. (2017) to investigate the quenching histories of group galaxies.

Briefly, we assume a flat prior on all the model parameters and model the difference between the observed and predicted $u-r$ and $NUV-u$ colours as independent realisations of a double Gaussian likelihood function (Equation 2 in Smethurst et al. 2015). An example posterior probability distribution output by STARPY is shown for a single galaxy in Figure 5 of Smethurst et al. (2015), wherein the degeneracies of the SFH model between recent, rapid quenching and earlier, slower quenching can be seen.

To study the SFH across a sample of many galaxies, these individual posterior probability distributions are stacked in $[t_q, \tau]$ space to give a single distribution for the sample. This is no longer inference but merely a method to visualise the results for a population of galaxies (see appendix section C in Smethurst et al. 2016 for a discussion on alternative methods which may be used to determine the parent population SFH). These distributions will be referred to as the population SFH densities.

## 3 RESULTS

We determine the population SFH densities for both the fast and slow rotators of the MM-Q-MANGA-GALEX sample. This is shown in Figure 4 for both the onset time (left panel) and exponential rate (right panel) of quenching for the fast (black solid line) and slow (red dashed line) rotators. Uncertainties on the population densities (shown by the shaded regions) are determined from the maximum and minimum values spanned by $N = 1000$ bootstrap iterations, each sampling 90% of either the fast (black shaded region) or slow (red shaded region) rotators.

To statistically test the significance of our results, we estimate the 'best fit' $[t_q, \tau]$ values for each galaxy with the median value of an individual galaxy's posterior probability distribution from STARPY (i.e. the 50th percentile position of the MCMC chain). We test the distribution of these values of the fast and slow rotators in the MM-Q-MANGA-GALEX sample with AD-tests. Firstly, an AD-test on the distributions of $t_q$ values in the fast and slow rotator samples, revealed that we cannot reject the null hypothesis that the fast and slow rotators quench at the same time ($AD = 0.9$, $p = 0.1$). Finally, an AD-test on the distributions of $\tau$ values, revealed that we can reject the null hypothesis that the fast and slow rotators quench at the same rate ($AD = 4.4$, $p = 0.006$)[4]. This is a $2.9\sigma$ result and suggests that slow rotators quench faster than fast rotators of the same mass.

## 4 DISCUSSION

The results presented in Section 3 suggest that fast and slow rotators are indeed separate populations quenched, and therefore formed, by different mechanisms. However, these quenching mechanisms occur at statistically indistinguishable onset times for fast and slow rotators, despite noticeable differences in the population densities, particularly at recent quenching times (see left panel of Figure 4). Khochfar et al. (2011) find in their simulations that the last major merger interaction for slow rotators was at $z \gtrsim 1.5$ (i.e. $t_q \lesssim 4.5$ Gyr). Whereas Penoyre et al. (2017) find in the Illustris simulation that slow rotators only form after $z < 1$ (i.e. $t_q \gtrsim 6$ Gyr). We note that STARPY is not very sensitive to the time of quenching, particularly at early times ($t_q \lesssim 6$ Gyr when $z \gtrsim 1$), due to the degeneracies between the optical and NUV colours currently used to infer the quenching parameters. Therefore, we cannot currently conclude which scenario our results favour. Future work altering our inference code to take spatial spectral information provided by MaNGA may help us to address this issue by breaking the degeneracies inherent in the photometric colours.

However, STARPY in its current form is sensitive to the rate of quenching in a galaxy. In the right panel of Figure 4 we see that there is a wide range of quenching rates occurring within the fast rotator sample. Previous works using STARPY have shown how the intermediate quenching rates ($1 \lesssim \tau$ [Gyr] $\lesssim 2$) prevalent in the distribution of the fast rotator sample can be attributed to environmental processes such as harassment and galaxy interactions (Smethurst et al. 2017), or minor mergers (Smethurst et al. 2015).

In particular we find evidence for galaxies in the fast rotator sample to quench at slow rates ($\tau \geqslant 2$ Gyr). Since the Q-MANGA-GALEX sample is agnostic to visual morphology, it will contain fast rotators which are disc dominated (i.e. late-type galaxies). This preference for slow quenching rates is therefore likely to be caused by the effects of secular evolution through morphological quenching, slowly moving these disc galaxies off the SFS to produce the red spiral population of Masters et al. (2012). Using the morphological classifications of Galaxy Zoo 2 (GZ2 Lintott et al. 2011; Willett et al. 2013) we find that 20 of the fast rotators of

[4] We also tested the distributions of the colours of the slow and fast rotators in the MM-Q-MANGA-GALEX sample and found that both the $u-r$ ($AD = 6.3$, $p = 0.001$) and NUV-u ($AD = 18.1$, $p = 9 \times 10^{-6}$) colours of the two kinematic classifications are statistically distinguishable.

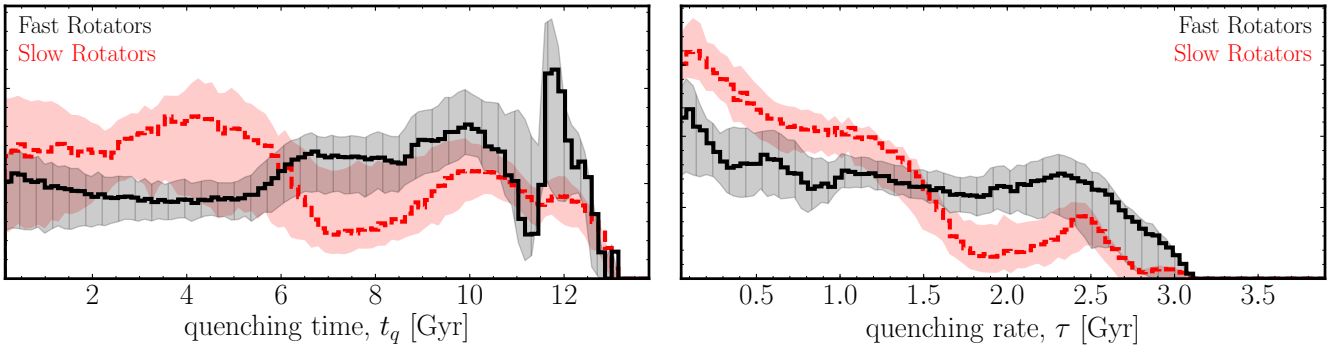


**Figure 4.** Population densities for the time, $t_q$ (left) and exponential rate, $\tau$ (right) that quenching occurs in the MM-Q-MANGA-GALEX sample for the fast (black, solid) and slow (red, dashed) rotators. A high value of $t_q$ corresponds to a recent quench, and a high value of $\tau$ corresponds to a slow quench. Shaded regions show the uncertainties on the distributions from bootstrapping.

the MM-Q-MANGA-GALEX sample are disc dominated with a disc or featured debiased vote fraction, $p_d \geqslant 0.8$ (i.e. 80% of classifiers marked the galaxy as having either a disc or features). This is consistent with the fact that $27\ ^{+1}_{-9}$ % of the fast rotator quenching rate population density (black line in the right panel of Figure 4) is found at quenching rates $\tau > 2$ Gyr.

Conversely only 1 of the slow rotators was classified as having a disc or features by GZ2. Upon visual inspection this galaxy has a large disc with spiral structure lying outside of the MaNGA fibre bundle at $> 1.5$ $R_e$. It is not surprising therefore, that there is much less preference for slow quenching rates, with $\tau \geqslant 2$ Gyr, for slow rotators than fast rotators in the right panel of Figure 4. However, Smethurst et al. (2015) found for galaxies in the red sequence visually classified as 'smooth' in GZ2 (i.e. quenching or quenched early-types) that a significant fraction, 26.1%, of the quenching rate population density was found at these slow quenching rates (see left panel of their Figure 8). However, a sample of visual classified 'smooth' galaxies in GZ2 may include both fast and slow rotators. It is only in this work that we have been able to investigate the difference in the SFHs of galaxies which are truly dispersion dominated from those which are rotationally supported.

These dispersion dominated galaxies in the Q-MANGA-GALEX sample instead show a preference for rapid quenching rates ($\tau \lesssim 1$ Gyr) in the right panel of Figure 4. This supports the theory that these galaxies are formed by major mergers which, along with destroying the disc of a galaxy, are thought to cause quenching at such rapid rates (Springel et al. 2005; Bell et al. 2006; Lotz et al. 2008, 2011; Smethurst et al. 2015). Surprisingly, we also find evidence that some of the fast rotators are quenching at these same rapid rates ($\tau \lesssim 1$ Gyr) in the right panel of Figure 4. This suggests that in a fraction of fast rotators a major merger may be the cause of quenching.

Simulations have recently shown that although major mergers (2:1 or 1:1 mergers) can cause rapid quenching of a galaxy, they do not necessarily destroy the disc dominated nature of a galaxy (Pontzen et al. 2016; Sparre & Springel 2016) and can actually form a fast rotator remnant (Bois et al. 2011). This is thought to mainly occur in gas rich major mergers (Bois et al. 2011) and is likely the explanation for the preference for rapid rates in the fast rotator sample seen in the right panel of Figure 4. There are currently ongoing follow-up observations using the Green Bank Telescope (GBT16A-095 and GBT17A-012; Masters et al. *in prep.*) to obtain HI profiles for galaxies in the MaNGA target sample. This data will allow us to test whether the fast rotators are indeed more gas rich than the slow rotators in this sample and therefore determine whether gas mass has an impact on the formation mechanisms of these kinematically distinct galaxies.

## 5 CONCLUSIONS

We have investigated the star formation histories of quenching or quenched fast and slow rotators identified in the MaNGA galaxy sample, irrespective of their visual morphology. We used the $u-r$ and $NUV-u$ colours with an existing piece of inference software, STARPY, to determine the onset time and exponential rate of quenching in each of these galaxies.

We find that rapid quenching rates ($\tau \lesssim 1$ Gyr) are more prevalent for slow rotators than fast rotators, with an Anderson-Darling test revealing that the two distributions are statistically distinguishable ($p = 0.006$, $2.9\sigma$). These rapid quenching rates found for slow rotators support the theory that fast rotators form in major mergers. Conversely, we find that fast rotators quench at a much wider range of rates, consistent with secular evolution, minor mergers, gas accretion and environmentally driven mechanisms. However we also find evidence that some of the fast rotators are quenching at the same rapid rates as the slow rotator sample.

This finding of rapid quenching rates occurring for both slow rotators and a subset of the fast rotators suggests that although their kinematics are different in nature, both classes of galaxy may be able to quench, and therefore form, via major mergers. This result combined with the findings of recent simulations showing disc survival in gas-rich major mergers (Bois et al. 2011; Pontzen et al. 2016; Sparre & Springel 2016), suggests that the total gas mass fraction within a pair of merging galaxies, is what will ultimately decide the kinematic fate of a galaxy.

**ACKNOWLEDGEMENTS**

RJS gratefully acknowledges research funding from the Ogden Trust. AW acknowledges support of a Leverhulme Trust Early Career Fellowship

Funding for the Sloan Digital Sky Survey IV has been provided by the Alfred P. Sloan Foundation, the U.S. Department of Energy Office of Science, and the Participating Institutions. SDSS acknowledges support and resources from the Center for High-Performance Computing at the University of Utah. The SDSS web site is `www.sdss.org`.

SDSS is managed by the Astrophysical Research Consortium for the Participating Institutions of the SDSS Collaboration including the Brazilian Participation Group, the Carnegie Institution for Science, Carnegie Mellon University, the Chilean Participation Group, the French Participation Group, Harvard-Smithsonian Center for Astrophysics, Instituto de Astrofísica de Canarias, The Johns Hopkins University, Kavli Institute for the Physics and Mathematics of the Universe (IPMU) / University of Tokyo, Lawrence Berkeley National Laboratory, Leibniz Institut fr Astrophysik Potsdam (AIP), Max-Planck-Institut für Astronomie (MPIA Heidelberg), Max-Planck-Institut fr Astrophysik (MPA Garching), Max-Planck-Institut für Extraterrestrische Physik (MPE), National Astronomical Observatories of China, New Mexico State University, New York University, University of Notre Dame, Observatório Nacional / MCTI, The Ohio State University, Pennsylvania State University, Shanghai Astronomical Observatory, United Kingdom Participation Group, Universidad Nacional Autónoma de México, University of Arizona, University of Colorado Boulder, University of Oxford, University of Portsmouth, University of Utah, University of Virginia, University of Washington, University of Wisconsin, Vanderbilt University and Yale University.

**REFERENCES**

Abazajian K. N. et al., 2009, ApJS, 182, 543
Abolfathi B. et al., 2017, ArXiv e-prints, 1707.09322
Aguerri J. A. L., González-García A. C., 2009, A&A, 494, 891
Bamford S. P. et al., 2009, MNRAS, 393, 1324
Bell E. F., Phleps S., Somerville R. S., Wolf C., Borch A., Meisenheimer K., 2006, ApJ, 652, 270
Blanton M. R., Eisenstein D., Hogg D. W., Schlegel D. J., Brinkmann J., 2005, ApJ, 629, 143
Blanton M. R., Roweis S., 2007, AJ, 133, 734
Bois M. et al., 2011, MNRAS, 416, 1654
Brinchmann J., Charlot S., White S. D. M., Tremonti C., Kauffmann G., Heckman T., Brinkmann J., 2004, MNRAS, 351, 1151
Bruzual G., Charlot S., 2003, MNRAS, 344, 1000
Bundy K. et al., 2015, ApJ, 798, 7
Cappellari M., 2016, ARA&A, 54, 597
Cappellari M. et al., 2007, MNRAS, 379, 418
Cappellari M. et al., 2011, MNRAS, 413, 813
Cappellari M. et al., 2013, MNRAS, 432, 1862
Cardelli J. A., Clayton G. C., Mathis J. S., 1989, ApJ, 345, 245
Chabrier G., 2003, PASP, 115, 763
D'Eugenio F., Houghton R. C. W., Davies R. L., Dalla Bontà E., 2013, MNRAS, 429, 1258
Drory N. et al., 2015, AJ, 149, 77
Duc P.-A. et al., 2011, MNRAS, 417, 863
Emsellem E. et al., 2011, MNRAS, 414, 888
Emsellem E. et al., 2007, MNRAS, 379, 401
Fang J. J., Faber S. M., Koo D. C., Dekel A., 2013, ApJ, 776, 63
Foreman-Mackey D., Hogg D. W., Lang D., Goodman J., 2013, PASP, 125, 306
Gunn J. E. et al., 2006, AJ, 131, 2332
Hayward C. C., Torrey P., Springel V., Hernquist L., Vogelsberger M., 2014, MNRAS, 442, 1992
Hopkins P. F., Hernquist L., Cox T. J., Kereš D., 2008, ApJS, 175, 356
Houghton R. C. W. et al., 2013, MNRAS, 436, 19
Jarosik N. et al., 2011, ApJS, 192, 14
Johnston E. J., Aragón-Salamanca A., Merrifield M. R., 2014, MNRAS, 441, 333
Kauffmann G. et al., 2003, MNRAS, 341, 33
Khochfar S. et al., 2011, MNRAS, 417, 845
Knebe A., Power C., Gill S. P. D., Gibson B. K., 2006, MNRAS, 368, 741
Law D. R. et al., 2016, AJ, 152, 83
Law D. R. et al., 2015, AJ, 150, 19
Lintott C. et al., 2011, MNRAS, 410, 166
Lotz J. M., Jonsson P., Cox T. J., Croton D., Primack J. R., Somerville R. S., Stewart K., 2011, ApJ, 742, 103
Lotz J. M., Jonsson P., Cox T. J., Primack J. R., 2008, MNRAS, 391, 1137
Martig M., Bournaud F., Teyssier R., Dekel A., 2009, ApJ, 707, 250
Martin D. C. et al., 2005, ApJ, 619, L1
Martin D. C. et al., 2007, ApJS, 173, 342
Masters K. L. et al., 2012, MNRAS, 424, 2180
Naab T. et al., 2014, MNRAS, 444, 3357
Noeske K. G. et al., 2007, ApJ, 660, L43
Oh K., Sarzi M., Schawinski K., Yi S. K., 2011, ApJS, 195, 13
Padmanabhan N. et al., 2008, ApJ, 674, 1217
Peng Y.-j. et al., 2010, ApJ, 721, 193
Penoyre Z., Moster B. P., Sijacki D., Genel S., 2017, ArXiv e-prints, 1703.00545
Pontzen A., Tremmel M., Roth N., Peiris H. V., Saintonge A., Volonteri M., Quinn T., Governato F., 2016, ArXiv e-prints, 1607.02507
Schawinski K. et al., 2014, MNRAS, 440, 889
Scott N., Davies R. L., Houghton R. C. W., Cappellari M., Graham A. W., Pimbblet K. A., 2014, MNRAS, 441, 274
SDSS Collaboration et al., 2016, ArXiv e-prints, 1608.02013
Smee S. A. et al., 2013, AJ, 146, 32
Smethurst R. J., Lintott C. J., Bamford S. P., Hart R. E., Kruk S. J., Masters K. L., Nichol R. C., Simmons B. D., 2017, ArXiv e-prints, 1704.06269
Smethurst R. J. et al., 2016, MNRAS, 463, 2986
Smethurst R. J. et al., 2015, MNRAS, 450, 435
Snyder G. F., Cox T. J., Hayward C. C., Hernquist L., Jonsson P., 2011, ApJ, 741, 77
Sparre M., Springel V., 2016, ArXiv e-prints, 1610.03850
Springel V., Di Matteo T., Hernquist L., 2005, ApJ, 620, L79

Stott J. P. et al., 2016, MNRAS, 457, 1888
Stoughton C. et al., 2002, AJ, 123, 485
Toloba E. et al., 2015, ApJ, 799, 172
Toomre A., Toomre J., 1972, ApJ, 178, 623
Veale M. et al., 2017, MNRAS, 464, 356
Wake D. A. et al., 2017, ArXiv e-prints, 1707.02989
Weiner B. J. et al., 2006, ApJ, 653, 1049
Willett K. W. et al., 2013, MNRAS, 435, 2835
Yan R. et al., 2016, AJ, 152, 197
Yang X., Mo H. J., van den Bosch F. C., 2009, ApJ, 695, 900
York D. G. et al., 2000, AJ, 120, 1579